Engineering 12 (2022) 55–61

Contents lists available at ScienceDirect

Engineering

journal homepage: www.elsevier.com/locate/eng

Research
Material Science and Engineering—Article

Current-Induced Magnetic Switching in an $L1_0$ FePt Single Layer with Large Perpendicular Anisotropy Through Spin–Orbit Torque

Kaifeng Dong [a,b], Chao Sun [a,b], Laizhe Zhu [a,b], Yiyi Jiao [a,b], Ying Tao [a,b], Xin Hu [a,b], Ruofan Li [c], Shuai Zhang [c], Zhe Guo [c], Shijiang Luo [c], Xiaofei Yang [c], Shaoping Li [d], Long You [c,e,f,*]

[a] School of Automation, China University of Geosciences, Wuhan 430074, China
[b] Hubei Key Laboratory of Advanced Control and Intelligent Automation for Complex Systems, China University of Geosciences, Wuhan 430074, China
[c] School of Optical and Electronic Information, Huazhong University of Science and Technology, Wuhan 430074, China
[d] China Resources Microelectronics Limited, Shanghai 200072, China
[e] Shenzhen Huazhong University of Science and Technology Research Institute, Shenzhen 518000, China
[f] Wuhan National High Magnetic Field Center, Huazhong University of Science and Technology, Wuhan 430074, China

ARTICLE INFO

Article history:
Received 16 July 2020
Revised 1 September 2021
Accepted 12 September 2021
Available online 03 January 2022

Keywords:
$L1_0$ FePt
SOT
Inversion asymmetry
Magnetic switching
Perpendicular anisotropy

ABSTRACT

In this study, current-induced partial magnetization-based switching was realized through the spin–orbit torque (SOT) in single-layer $L1_0$ FePt with a perpendicular anisotropy ($K_{u\perp}$) of 1.19×10^7 erg·cm^{-3} (1 erg·cm^{-3} = 0.1 J·m^{-3}), and its corresponding SOT efficiency (β_{DL}) was 8×10^{-6} Oe·(A·cm^{-2})$^{-1}$ (1 Oe = 79.57747 A·m^{-1}), which is several times higher than that of the traditional Ta/CoFeB/MgO structure reported in past work. The SOT in the FePt films originated from the structural inversion asymmetry in the FePt films since the dislocations and defects were inhomogeneously distributed within the samples. Furthermore, the FePt grown on MgO with a granular structure had a larger effective SOT field and efficiency than that grown on $SrTiO_3$ (STO) with a continuous structure. The SOT efficiency was found to be considerably dependent on not only the sputtering temperature-induced chemical ordering but also the lattice mismatch-induced evolution of the microstructure. Our findings can provide a useful means of efficiently electrically controlling a magnetic bit that is highly thermally stable via SOT.

1. Introduction

A simple and efficient means of reorienting the magnetization of films with high magnetic anisotropy energy is highly desirable for further advancement of modern information technologies [1,2]. Compared with magnetization switching by a magnetic field, current-induced spin torque switching enables higher storage density, faster writing speed, and lower energy consumption [3,4]. The electrical manipulation of the magnetization in ferromagnetic (FM) nanostructures through current-induced spin–orbit torque (SOT) is one of the representative phenomena based on spin–orbit coupling (SOC) and has recently attracted considerable attention as a new route for magnetization switching [5–10]. In general, SOT is recognized as a spin transfer torque originating from a spin current (J_s) converted from a charge current via spin–orbit effects, such as the spin Hall effect (SHE) and Rashba–Edelstein effect [11–13]. FePt in the $L1_0$ phase possesses one of the highest perpendicular magnetocrystalline anisotropies among transition metal compounds, which enables memory cells with sufficient thermal stability to be scaled down to 5 nm [14,15]. However, reversing the magnetization of $L1_0$ FePt is extremely challenging. Although different strategies, such as energy-assisted magnetic recording, voltage control, and probe-based spin injection, have been proposed to ease the magnetization switching of $L1_0$ FePt, major issues regarding reliability, compatibility, and efficiency prevent practical applications. If we examine the mechanism of the high magnetic anisotropy of $L1_0$ FePt, it mainly originates from the strong coupling between the spin and orbital angular momenta and hybridization between Pt 5d and Fe 3d electrons. SOC is also the premise of the recently discovered SOT effect, which opens new avenues for the possible electrical manipulation of the magnetization of $L1_0$ FePt. A few recent works demonstrated current-induced perpendicular magnetization switching in an $L1_0$ FePt single layer [16–19]. These findings could become a guide toward a method for highly efficient SOT switching of magnetic materials with high

* Corresponding author.
E-mail address: lyou@hust.edu.cn (L. You).

https://doi.org/10.1016/j.eng.2021.09.018

anisotropy energy. However, the effect of the microstructure on the SOT properties has not been systematically investigated. Actually, different microstructures would induce different perpendicular anisotropies and chemical ordering, thus causing discrepancies in the SOT properties. How the microstructure of FePt films affects the SOT properties must be clarified in detail. For this purpose, in this work, current-induced SOT switching of magnetization is realized in a FePt single layer. The effective fields of patterned FePt films grown on different substrates with different growth temperatures are systematically investigated. With varying growth temperature and substrate, perpendicularly magnetized FePt films with different microstructures are achieved. We find that the SOT efficiency in a FePt single layer dramatically depends on the microstructure of the films.

2. Experiments

Four types of samples with different film growth temperatures and substrates were used: FePt 10 nm (300 °C)/MgO substrate (Sample I), FePt 10 nm (400 °C)/MgO substrate (Sample II), FePt 10 nm (500 °C)/MgO substrate (Sample III), and FePt 10 nm (400 °C)/$SrTiO_3$ (STO) substrate (Sample IV). The films were deposited using an ultrahigh vacuum magnetron sputtering system, and their stack is shown in Fig. 1(a). They were then patterned into a Hall bar microstructure of a 20–45 μm length, with a 15 μm wide path for the flow of current and a 6 μm wide path for voltage detection, using ultraviolet lithography followed by argon ion etching. Pt electrodes were deposited at the four ends of the Hall bar to facilitate electrical measurement. We assigned the same serial number to the device as the corresponding sample from which it had been fabricated. Fig. 1(b) illustrates a schematic of the devices showing the schematic of the Hall bar structure with the definition of the coordinate system, and Fig. 1(c) shows an optical image of a device. Anomalous Hall effect (AHE) and current-induced magnetization switching measurements were performed using a homemade setup with a Keithley 2602B (USA) as a current-source meter and a Keithley 2182 as a nanovoltage meter. The pulse duration was set as 12 ms. A small current (100 μA) was applied after each pulse current to measure the anomalous Hall resistance (R_H). The effective SOT fields of the devices were measured by a harmonic voltage analysis system. During measurement, a low-frequency alternating current (AC) was applied to the current path of the Hall bar. The AC frequency was 317.3 Hz. The external trigger function of the phase generator of the current source was used to lock the input channel and reference channel of the lock-in amplifier. The voltage path of the Hall bar was connected to two lock-in amplifiers to measure the first and second components of the harmonic Hall voltage. Microstructure characterization of the films and energy-dispersive X-ray (EDX, Bruker super-X EDS, Germany) composition mapping were performed by using a transmission electron microscope (TEM, FEI Titan Themis 200 TEM, USA).

3. Results and discussion

Fig. 1(d) shows the AHE measurements of patterned 400 °C FePt 10 nm/MgO and FePt 10 nm/STO films. Both patterned films exhibited excellent perpendicular anisotropy. The M–H loops (Figs. 1(e) and (f)) of the films were consistent with the AHE results. The low-magnification cross-sectional TEM image revealed that the FePt

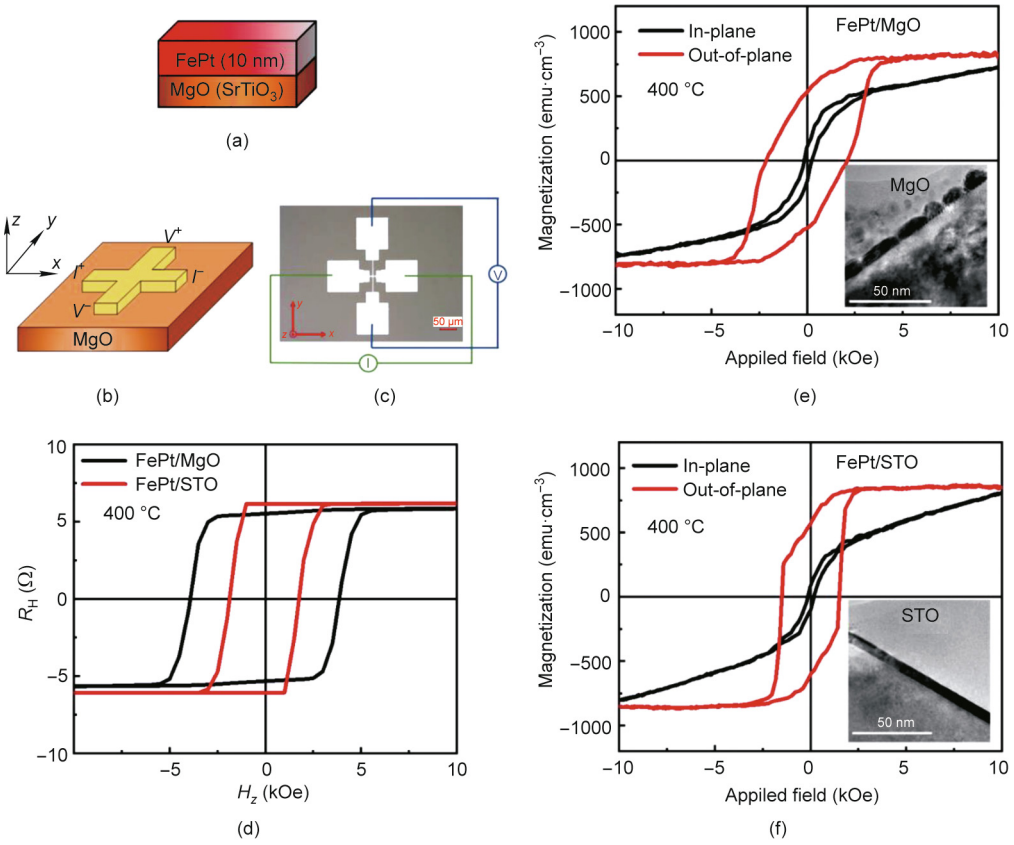

Fig. 1. (a) Film stack structure; (b) schematic of a Hall bar with the coordinate system; (c) optical microscope image of a device; (d) AHE loops of FePt 10 nm/MgO and FePt 10 nm/STO films; (e, f) M–H loops of (e) FePt 10 nm/MgO and (f) FePt 10 nm/STO films. All the films were grown at the temperature of 400 °C. The inserts in (e) and (f) show the corresponding low-magnification cross-sectional TEM images. 1 Oe = 79.57747 A·m^{-1}; 1 emu·cm^{-3} = 1 × 10^3 A·m^{-1}.

films grown on MgO had an island structure (insert in Fig. 1(e)), while the FePt films grown on STO had a continuous structure (insert in Fig. 1(f)). Moreover, the perpendicular anisotropy ($K_{u\perp}$) can be calculated from $K_{u\perp} = M_s H_k/2 + 2\pi M_s^2$, where M_s is saturated magnetization, H_k is the magnetic anisotropy field (estimated by extrapolating the hard axis loop). The calculated $K_{u\perp}$ values were 9.8×10^6 erg·cm^{-3} (1 erg·cm^{-3} = 0.1 J·m^{-3}) (MgO) and 9.4×10^6 erg·cm^{-3} (STO), as shown in Table 1, which were much larger than those reported for SOT devices using other materials, such as CoFeB [6,7], Co [8–10], CoNi [11], and CoFe [12]. FePt films grown on MgO had better chemical ordering and perpendicular anisotropy than those grown on STO, which can be attributed to lattice mismatch-induced microstructural evolution [20].

The current-induced magnetization switching in samples (Samples II and IV) made from 400 °C FePt 10 nm/MgO and FePt 10 nm/STO films with different external in-plane fields (H_x), ranging from −1000 to 1000 Oe (1 Oe = 79.57747 A·m^{-1}), is shown in Fig. 2. Here, H_x is used to break the torque symmetry. To clarify the switching evolution, we use the red eight-pointed star symbols to denote the initial states of magnetization and arrows to show the switching direction in Fig. 2. Partial magnetization switching was achieved by sweeping the pulsed current in both devices. These results show that current-induced partial magnetization switching can be realized in materials with high anisotropy energy (high perpendicular anisotropy and thick magnetic films). Moreover, the polarity of the switching loop reversed once the external magnetic field was reversed, and switching did not occur without an external magnetic field. This phenomenon is a typical SOT-induced switching behavior similar to that found in heavy-metal (HM)/FM bilayers, which agrees with the results of previous work [16]. The switching ratio ρ_{sw} was 2.5% and 3.2% under H_{opt} about 500 Oe on the MgO substrate (Sample II, Fig. 2(a)) and about 1000 Oe on the STO substrate (Sample IV, Fig. 2(b)), respectively. Here, ρ_{sw} is defined as the ratio of $\Delta R_l/\Delta R_H$ (ΔR_l represents the AHE resistance variation during current-induced switching, ΔR_H represents the AHE resistance variation during out-of-plane field sweeping), H_{opt} is the optimum applied in-plane field. For films grown on the STO substrate, a larger H_x (above 200 Oe) was required for magnetization switching compared to those grown on the MgO substrate. The switching ratio ρ_{sw} is smaller than those reported in previous works [16,18,19]. In the work of Tang et al. [19], the maximal switching ratio was approximately 24% for 4 nm thick FePt films. Moreover, the switching ratio was found to be affected by the FePt film thickness (4–220 nm). The thinner the FePt film was, the larger the switching ratio. However, in the work of Liu et al. [16], FePt 6 nm and FePt 20 nm appeared to have similar switching ratios of 20%, which were not dependent on the FePt thickness. Furthermore, Zheng et al. [18] found that the

Table 1
Summary of the $I_{(001)}/I_{(002)}$, out-of-plane coercivity $H_{c\perp}$, magnetic anisotropy field H_k, saturated magnetization M_s, perpendicular anisotropy $K_{u\perp}$, and SOT efficiency β_{DL} of the four FePt films.

Sample	$I_{(001)}/I_{(002)}$	$H_{c\perp}$ (kOe)	H_k (kOe)	M_s (emu·cm^{-3})	$K_{u\perp}$ ($\times 10^7$ erg·cm^{-3})	β_{DL} ($\times 10^{-6}$ Oe·(A·cm^{-2})$^{-1}$)
I	–	0.24	7.90	641	0.45	–
II	0.85	2.11	13.71	821	0.98	4.2
III	1.18	5.21	16.62	867	1.19	8.0
IV	0.52	1.55	11.18	861	0.94	1.3

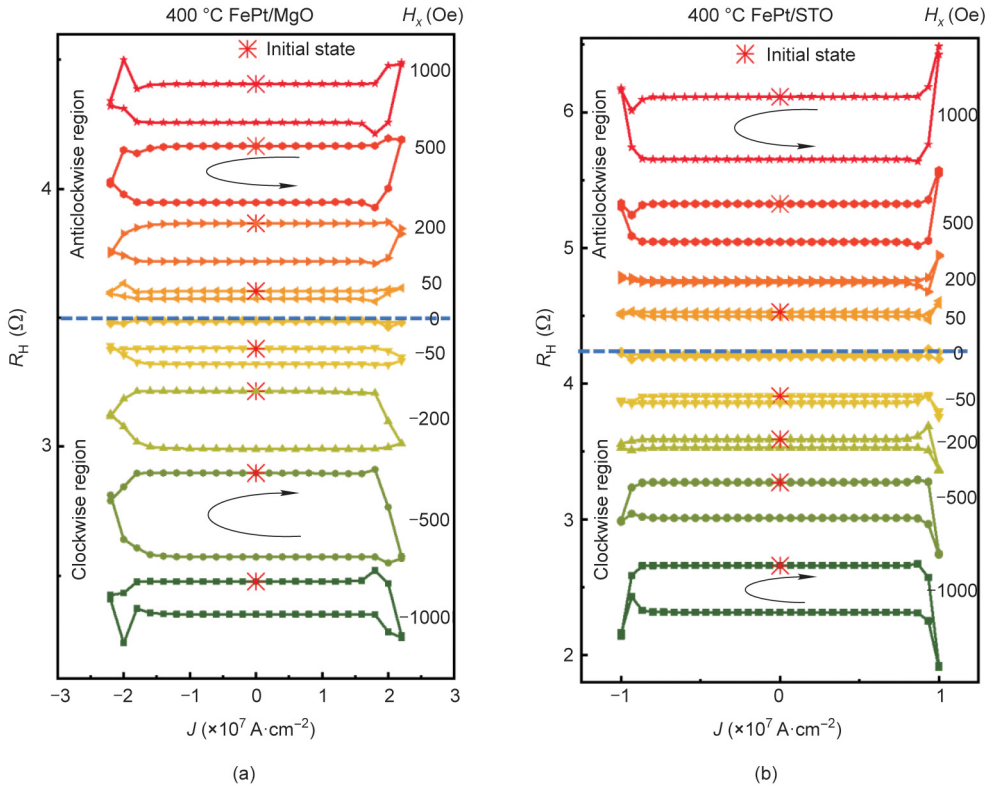

Fig. 2. Current-induced magnetization switching of FePt films with different external fields H_x for (a) FePt 10 nm/MgO and (b) FePt 10 nm/STO with a growth temperature of 400 °C.

switching ratio was strongly dependent on the chemical ordering, and a larger switching ratio could be obtained from a 3 nm thick FePt film with more disorder. The maximal switching ratio was approximately 88%. Based on the above works, the switching ratio, broadly speaking, is affected by several factors, namely the microstructure, magnetic properties, thickness, and so on, although some conclusions are not consistent. In addition, the imperfections in the Hall bar structure can also affect the switching ratio [21]. The reduced current density in the center of the Hall cross and the additional pinning from the magnetic Hall arms will also decrease the switching ratio. In addition, the critical switching current density (J_C), defined as the value of the electrical current density at which R_H begins to change (for up-to-down and down-to-up switching), of FePt films grown on the STO substrate was smaller than that of FePt films grown on the MgO substrate under the same applied in-plane field.

The harmonic Hall voltage was measured to quantitatively analyze the SOT efficiency of the samples (Fig. 3). Fig. 3(a) shows the measurement setup. As a representative example, Figs. 3(c)–(f) show the results of typical measurements of the first (V_ω) and second ($V_{2\omega}$) harmonic signals of the single-layer FePt/MgO prepared at 400 °C, where the applied magnetic field was swept along the x and y directions. The SOT was thought to feature a damping-like torque and a field-like torque, and the corresponding effective fields, ΔH_{DL} and ΔH_{FL}, were calculated by

$$\Delta H_{DL} = -\frac{2(B_x \pm 2\xi B_y)}{1-4\xi^2} \quad (1)$$

$$\Delta H_{FL} = -\frac{2(B_y \pm 2\xi B_x)}{1-4\xi^2} \quad (2)$$

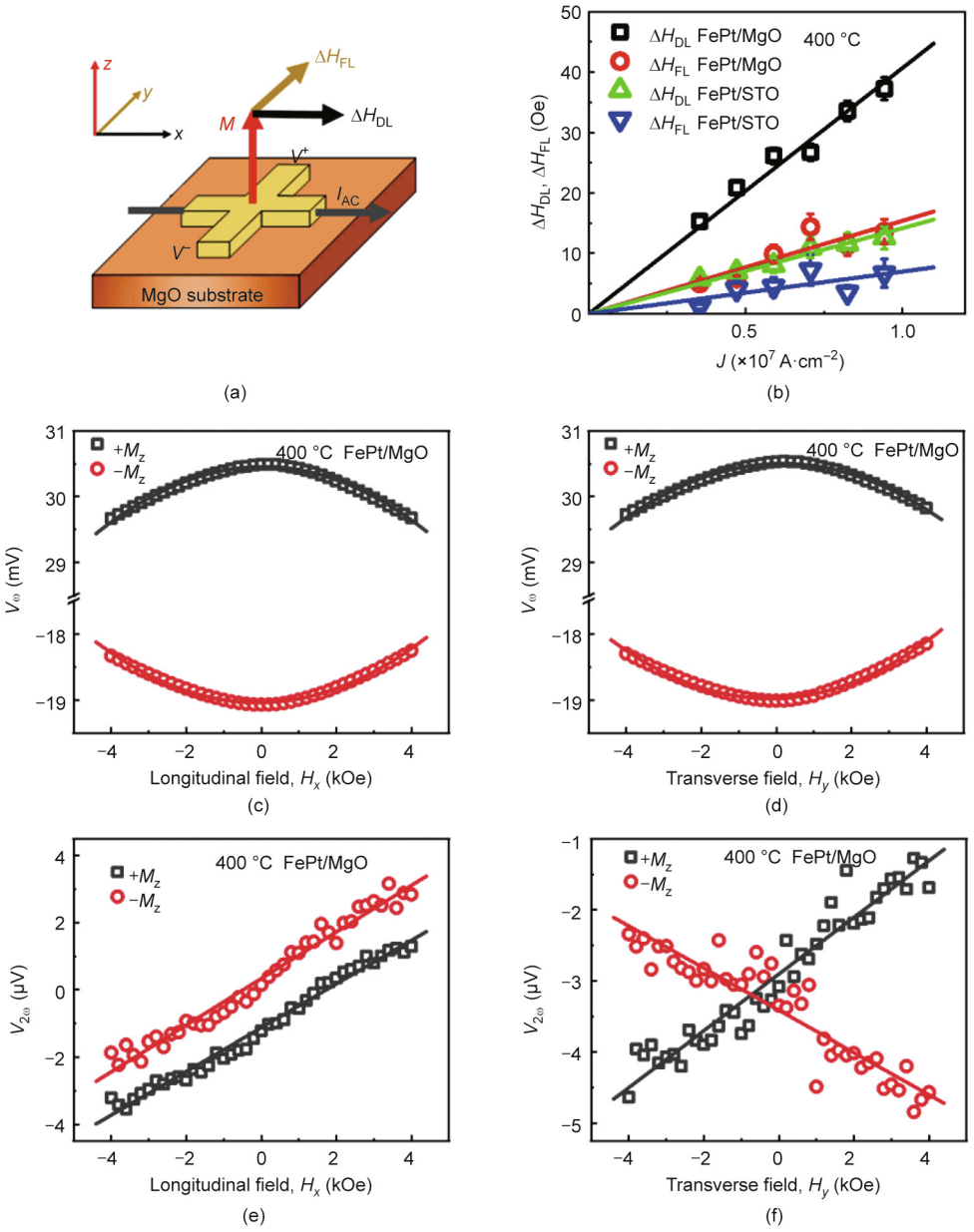

Fig. 3. (a) Schematic illustration of the spin–orbit effective field (ΔH_{DL} and ΔH_{FL}) in FePt films. (b) Summary of the SOT effective field at different current densities in FePt films. (c–f) In addition to typical harmonic Hall voltage measurement results for FePt 10 nm/MgO films with a growth temperature of 400 °C, magnetic field dependence of the (c, e) first and (d, f) second harmonic signals. The external magnetic fields H_x and H_y were swept along the (c, e) x direction and (d, f) y direction.

where $B_x = \left(\frac{\partial V_{2\omega}}{\partial H_x}\right) / \left(\frac{\partial^2 V_\omega}{\partial H_x^2}\right)$, $B_y = \left(\frac{\partial V_{2\omega}}{\partial H_y}\right) / \left(\frac{\partial^2 V_\omega}{\partial H_y^2}\right)$, and $\xi = \frac{R_P}{R_H}$ is the ratio of the planar Hall resistance (R_P) to the anomalous Hall resistance (R_H) of the sample [8,22]. Given that the planar Hall resistance of FePt is negligibly small (see Fig. S1 in Appendix A for details), ξ = 0 was set. The relationship between the effective SOT field and the AC density of the Hall devices made from 400 °C FePt 10 nm/MgO and FePt 10 nm/STO films is summarized in Fig. 3(b). The results show that an effective SOT field occurred in the two FePt samples, and ΔH_{DL} was larger than ΔH_{FL}, suggesting that the damping-like torque was dominant in the single-layer FePt. Moreover, the effective SOT field of the FePt films grown on the MgO substrate was larger than that of the films grown on the STO substrate (Fig. 3(b)). We further evaluated the SOT efficiency, β_{DL}, defined as $\Delta H_{DL}/J$. The β_{DL} values for the two devices were 4.2 × 10^{-6} Oe·(A·cm^{-2})$^{-1}$ (on the MgO substrate) and 1.3 × 10^{-6} Oe·(A·cm^{-2})$^{-1}$ (on the STO substrate). This verified the high SOT efficiency in $L1_0$ FePt. In the work of Liu et al. [16], the β_{DL} of 20 nm FePt films grown on STO, MgO, and TiN/MgO had similar values due to the same continuous structure of these three films. However, the β_{DL} values of 10 nm FePt films grown on STO and MgO had a very large discrepancy in our case due to the different microstructures of these two films. Thus, the lattice mismatch-induced microstructure could still affect the chemical ordering and consequently SOT efficiency. FePt films grown on the MgO substrate with a granular structure had larger values of ΔH_{DL}, ΔH_{FL}, and β_{DL} than those grown on the STO substrate with a continuous structure.

To systematically investigate the effect of chemical ordering on the SOT properties, FePt films grown on the MgO substrate with different sputtering temperatures were prepared. The AHE and M–H loops for samples grown at 300 °C (Sample I) and 500 °C (Sample III) are shown in Figs. 4(a)–(c). Reexamining the magnetic properties of samples grown at 400 °C (Sample II), we can see that films on the MgO substrate exhibited excellent perpendicular anisotropy when the sputtering temperature exceeded 400 °C. The FePt films with enormous disorder (300 °C, Sample I) had a larger Hall resistance R_H than the more ordered FePt films (400 °C, Sample II; 500 °C, Sample III) due to different coherent band mixing effects [17]. With increasing sputtering temperature, the intensities of the FePt(001), (002), and (003) peaks increased, and the intensity ratio $I_{(001)}/I_{(002)}$ increased ($I_{(001)}/I_{(002)}$ is about 0.85 for Sample II with a growth temperature of 400 °C, $I_{(001)}/I_{(002)}$ is about 1.18 for Sample III with a growth temperature of 500 °C), suggesting that the (001) texture and thereby the chemical ordering improved (see Fig. S2 in Appendix A for details). The calculated $K_{u\perp}$ also increased from 4.5 × 10^6 to 1.19 × 10^7 erg·cm^{-3} when the sputtering temperature increased from 300 to 500 °C. The improvement in the chemical ordering and the perpendicular anisotropy originated from the improved (001) texture with increasing sputtering temperature. Partial magnetization switching was also achieved by sweeping the pulsed current in Sample I and III, as shown in Figs. 4(d) and (e). The switching ratio ρ_{sw} was 0.8%, 2.5%, and 6.6% for Sample I, II, and III, respectively, under the optimum applied in-plane fields of H_{opt} about 500 Oe (Sample I and II) and about 1000 Oe (Sample III). In addition, the critical switching current densities J_C of the samples exhibited significant differences but were not monotonically related to the film growth temperature.

To clarify the effect of H_x on J_C, the J_C as a function of H_x for Sample I (300 °C on the MgO substrate) is summarized in Fig. 5(a). J_C clearly decreased with increasing H_x, similar to the results from Lee et al. [23]. The SOT effective fields at different current densities in 500 °C FePt 10 nm/MgO films were measured (see Fig. S3 in Appendix A for details) and are summarized in Fig. 5(b). The effective field of Sample I (300 °C) was not measured due to the imperfect perpendicular magnetic anisotropy. ΔH_{DL}, ΔH_{FL}, and β_{DL} (8 × 10^{-6} Oe·(A·cm^{-2})$^{-1}$) increased with increasing sputtering temperature. Note that the value of β_{DL} of 8 × 10^{-6} Oe·(A·cm^{-2})$^{-1}$ in the single-layer FePt on the MgO substrate prepared at 500 °C was also larger than that reported in previous work on FePt (6.5 × 10^{-6} Oe·(A·cm^{-2})$^{-1}$) [16]. Combining this result with the results in Table 1, the effective SOT can be seen to be strongly affected by the chemical ordering and perpendicular anisotropy, and FePt films with higher chemical ordering and perpendicular anisotropy had a larger SOT effective field and a highly efficient SOT.

To investigate the origin of the SOT in FePt, TEM measurements were carried out. Fig. 6(a) shows a high-magnification cross-

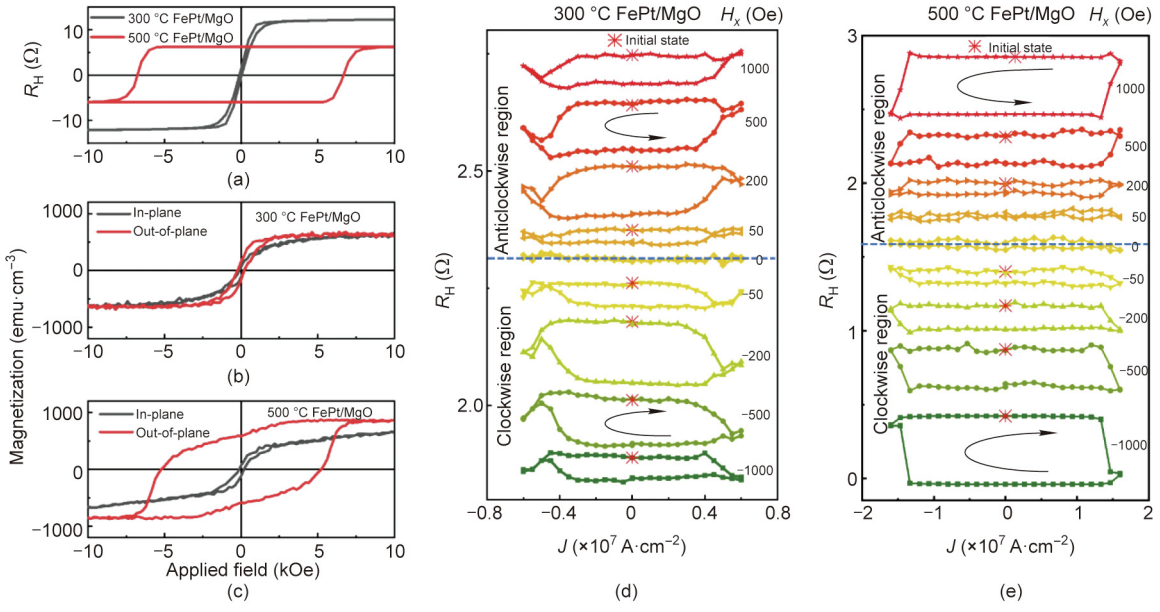

Fig. 4. (a) AHE loops of FePt 10 nm/MgO films with growth temperatures of 300 and 500 °C. (b, c) M–H loops of FePt 10 nm/MgO films with sputtering temperatures of (b) 300 °C and (c) 500 °C. Current-induced magnetization switching of FePt films with different external fields H_x for FePt 10 nm/MgO films with growth temperatures of (d) 300 °C and (e) 500 °C.

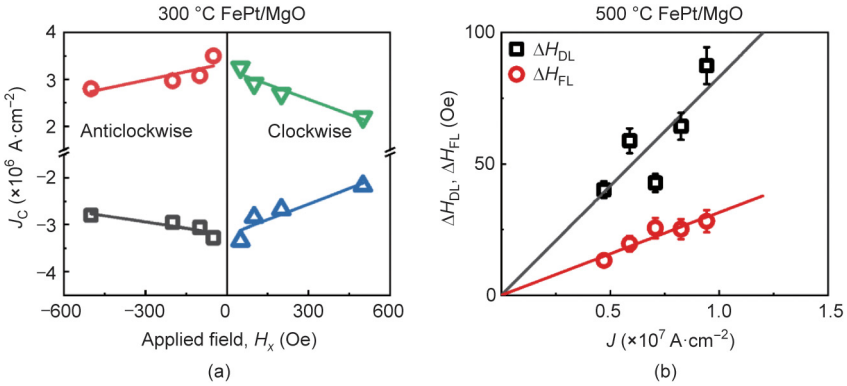

Fig. 5. (a) J_C as a function of H_x for the FePt 10 nm/MgO film with a growth temperature of 300 °C; (b) summary of the SOT effective field at different current densities in the FePt 10 nm/MgO film with a growth temperature of 500 °C.

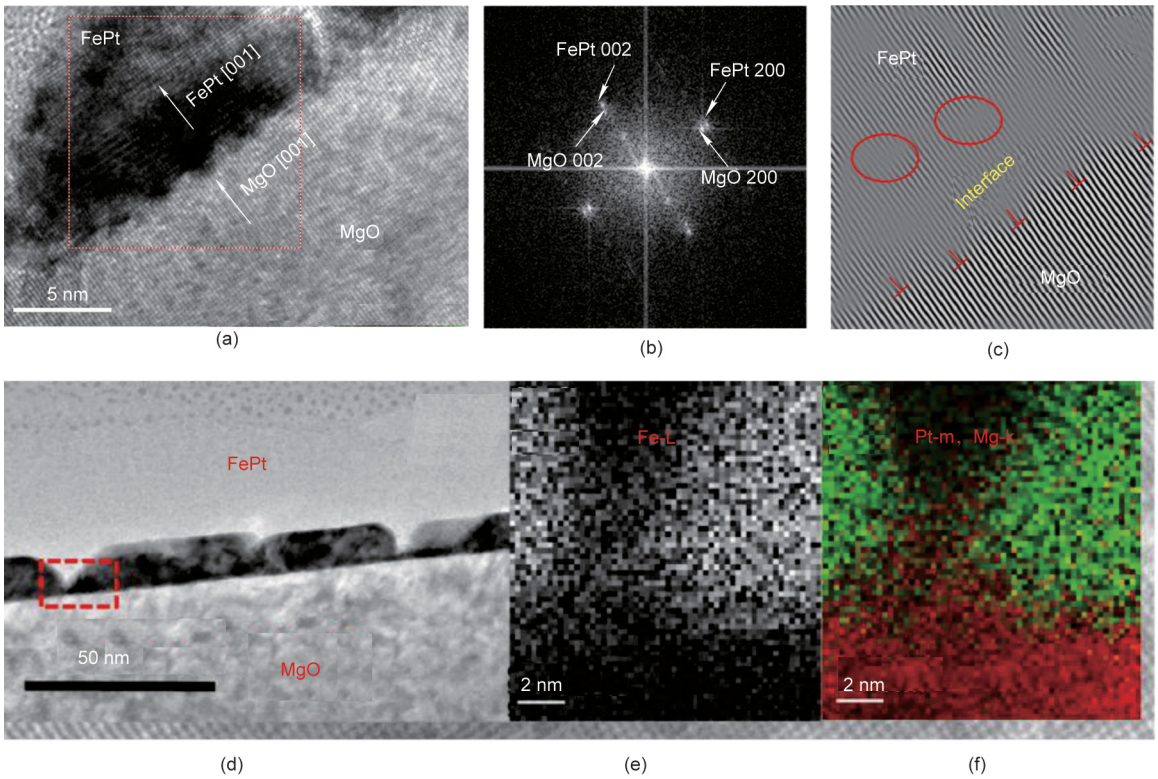

Fig. 6. For FePt 10 nm grown on the MgO substrate at a growth temperature of 500 °C: (a) high-resolution TEM cross-sectional image of the FePt and MgO layers; (b) corresponding SAED patterns of the FePt and MgO layers; (c) selected area inverse fast Fourier transform (IFFT) image; (d) low-magnification cross-sectional TEM image; and (e, f) selected area EDX mapping analyses of (e) Fe and (f) Pt and Mg atoms. L, m, and k represent different line series of X-ray.

sectional TEM image of single-layer FePt 10 nm/MgO prepared at 500 °C. (001) FePt grains were clearly epitaxially grown on the (200) textured MgO substrate. By combining these measurements with the corresponding selected area electron diffraction (SAED) patterns of FePt and MgO (Fig. 6(b)), the epitaxial relationship between them was confirmed to be FePt(001)<100>||MgO(001)<200>, similar to our previous results [20]. All these results indicate that the FePt films had good (001) texture. Moreover, dislocations at the interface were formed to release the strain energy (Fig. 6(c), marked as "⊥"). Furthermore, despite the good (001) texture, some defects were observed in the FePt films (Fig. 6(c), marked by red circles). Moreover, the FePt film grown on MgO had an island structure (Fig. 6(d)), different from that grown on STO [20]. This result was consistent with the results of the slope of the hysteresis loop in Fig. 1. The EDX mapping analyses of selected areas of the Fe, Pt, and Mg atoms are illustrated in Figs. 6(e) and (f). These results show that some Mg atoms diffused into the FePt films, which might have led to the formation of defects, as shown in Fig. 6(c). From recent reports, SOT can only be observed in magnetic materials with noncentrosymmetric space groups (bulk inversion asymmetry) or noncentrosymmetric site point groups (local structural inversion asymmetry) in crystal structures. In this study, $L1_0$ FePt grown on either a MgO or STO substrate could still be switched by an electric current. In our case, the dislocations and defects were inhomogeneously distributed within the samples (see Fig. S4 in Appendix A for details), which resulted in structural inversion asymmetry in the FePt films. Thus, SOT could be generated in the single-layer FePt.

4. Conclusion

In summary, we observed current-induced magnetic switching through SOT in an $L1_0$ FePt single layer. FePt films grown on MgO had larger perpendicular anisotropy and a larger SOT effective field than those grown on STO. The SOT efficiency was found to considerably depend on the chemical ordering and lattice mismatch-induced evolution of the microstructure. A high SOT efficiency of 8×10^{-6} Oe·(A·cm^{-2})$^{-1}$ was obtained for a 10 nm thick FePt layer with high perpendicular anisotropy, which implies its potential for use in magnetic memory and logic devices with high thermal stability and ultrahigh storage density. The investigation of the mechanism and performance of current-induced magnetization switching reported here should be pursued in future research in the field.

Acknowledgments

This work was supported by National Key Research and Development Program of China (2020AAA0109005), the National Natural Science Foundation of China (61674062, 51501168, 41574175, and 41204083), the Fundamental Research Funds for the Central Universities of the China University of Geosciences (Wuhan) (CUG150632 and CUGL160414), the Fundamental Research Funds for National Universities of the China University of Geosciences (Wuhan), the Interdisciplinary program of Wuhan National High Magnetic Field Center (WHMFC202119), Huazhong University of Science and Technology, and Fund from Shenzhen Virtual University Park (2021Szvup091).

Compliance with ethics guidelines

Kaifeng Dong, Chao Sun, Laizhe Zhu, Yiyi Jiao, Ying Tao, Xin Hu, Ruofan Li, Shuai Zhang, Zhe Guo, Shijiang Luo, Xiaofei Yang, Shaoping Li, and Long You declare that they have no conflict of interest or financial conflicts to disclose.

Appendix A. Supplementary data

Supplementary data to this article can be found online at https://doi.org/10.1016/j.eng.2021.09.018.

References

[1] Worledge DC, Hu G, Abraham DW, Sun JZ, Trouilloud PL, Nowak J, et al. Spin torque switching of perpendicular Ta|CoFeB|MgO-based magnetic tunnel junctions. Appl Phys Lett 2011;98(2):022501.
[2] Ramaswamy R, Lee JM, Cai K, Yang H. Recent advances in spin–orbit torques: moving towards device applications. Appl Phys Rev 2018;5(3):031107.
[3] Miron IM, Garello K, Gaudin G, Zermatten PJ, Costache MV, Auffret S, et al. Perpendicular switching of a single ferromagnetic layer induced by in-plane current injection. Nature 2011;476(7359):189–93.
[4] Liu L, Pai CF, Li Y, Tseng HW, Ralph DC, Buhrman RA. Spin–torque switching with the giant spin Hall effect of tantalum. Science 2012;336(6081):555–8.
[5] Liu L, Zhou C, Shu X, Li C, Zhao T, Lin W, et al. Symmetry-dependent field-free switching of perpendicular magnetization. Nat Nanotechnol 2021;16(3):277–82.
[6] Schulz T, Lee K, Krüger B, Lo Conte R, Karnad GV, Garcia K, et al. Effective field analysis using the full angular spin–orbit torque magnetometry dependence. Phys Rev B 2017;95(22):224409.
[7] Qiu X, Deorani P, Narayanapillai K, Lee KS, Lee KJ, Lee HW, et al. Angular and temperature dependence of current induced spin–orbit effective fields in Ta/CoFeB/MgO nanowires. Sci Rep 2015;4(1):4491.
[8] Garello K, Miron IM, Avci CO, Freimuth F, Mokrousov Y, Blügel S, et al. Symmetry and magnitude of spin–orbit torques in ferromagnetic heterostructures. Nat Nanotechnol 2013;8(8):587–93.
[9] Kong WJ, Ji YR, Zhang X, Wu H, Zhang QT, Yuan ZH, et al. Field-free spin Hall effect driven magnetization switching in Pd/Co/IrMn exchange coupling system. Appl Phys Lett 2016;109(13):132402.
[10] van den Brink A, Vermijs G, Solignac A, Koo J, Kohlhepp JT, Swagten HJM, et al. Field-free magnetization reversal by spin-Hall effect and exchange bias. Nat Commun 2016;7(1):10854.
[11] Fukami S, Zhang C, DuttaGupta S, Kurenkov A, Ohno H. Magnetization switching by spin–orbit torque in an antiferromagnet–ferromagnet bilayer system. Nat Mater 2016;15(5):535–41.
[12] Razavi SA, Wu D, Yu G, Lau YC, Wong KL, Zhu W, et al. Joule heating effect on field-free magnetization switching by spin–orbit torque in exchange-biased systems. Phys Rev Appl 2017;7(2):024023.
[13] Huang KF, Wang DS, Lin HH, Lai CH. Engineering spin–orbit torque in Co/Pt multilayers with perpendicular magnetic anisotropy. Appl Phys Lett 2015;107(23):232407.
[14] Hong J, Dong K, Bokor J, You L. Self-assembled single-digit nanometer memory cells. Appl Phys Lett 2018;113(6):062404.
[15] Chen JS, Hu JF, Lim BC, Lim YK, Liu B, Chow GM, et al. High coercive $L1_0$ FePt–C (001) nanocomopsite films with small grain size for perpendicular recording media. J Appl Phys 2008;103(7):07F517.
[16] Liu L, Yu J, González-Hernández R, Li C, Deng J, Lin W, et al. Electrical switching of perpendicular magnetization in a single ferromagnetic layer. Phys Rev B 2020;101(22):220402.
[17] Sato T, Seki T, Kohda M, Ryu J, Gamou H, Karube S, et al. Evaluation of spin–orbit torque in a $L1_0$-FePt single layer and a $L1_0$-FePt/Pt bilayer. Jpn J Appl Phys 2019;58(6):060915.
[18] Zheng SQ, Meng KK, Liu QB, Chen JK, Miao J, Xu XG, et al. Disorder dependent spin–orbit torques in $L1_0$ FePt single layer. Appl Phys Lett 2020;117(24):242403.
[19] Tang M, Shen Ka, Xu S, Yang H, Hu S, Lü W, et al. Bulk spin torque-driven perpendicular magnetization switching in $L1_0$ FePt single layer. Adv Mater 2020;32(31):2002607.
[20] Dong KF, Li HH, Chen JS. Lattice mismatch-induced evolution of microstructural properties in FePt films. J Appl Phys 2013;113(23):233904.
[21] Finley J, Lee CH, Huang PY, Liu L. Spin–orbit torque switching in a nearly compensated Heusler ferrimagnet. Adv Mater 2019;31(2):1805361.
[22] Hayashi M, Kim J, Yamanouchi M, Ohno H. Quantitative characterization of the spin–orbit torque using harmonic Hall voltage measurements. Phys Rev B 2014;89(14):144425.
[23] Lee KS, Lee SW, Min BC, Lee KJ. Threshold current for switching of a perpendicular magnetic layer induced by spin Hall effect. Appl Phys Lett 2013;102(11):112410.